Materials Advances

ROYAL SOCIETY OF CHEMISTRY

PAPER

View Article Online
View Journal | View Issue

Cite this: *Mater. Adv.*, 2025, **6**, 766

Development of a silver–polyaniline functionalized biosensor for non-enzymatic lactic acid detection

Vinay Kishnani,[a] Rahul Ashvinbhai Makadia,[a] Satheesh Natarajan,[b] Jayaraj Joseph[c] and Ankur Gupta *[a]

Sensor research based on biometal performance and health parameter detection attracts significant global interest in the biosensing community. In this study, an electrochemical biosensor has been developed for the detection of lactic acid (LA) in artificial saliva, and in this context, the screen-printed electrode was functionalized using a composite of silver nanoparticles (AgNPs) and silver nanoparticles–polyaniline (AgNPs–PANI). The cyclic voltammetry responses were recorded for non-enzymatic LA sensing. In this process, the electro-polymerization method has been used to generate a film of Ag–PANI on a screen-printed electrode (SPE). Several analytical techniques, including Fourier transform infrared spectroscopy (FTIR), ultraviolet-visible spectroscopy (UV-visible), field emission scanning electron microscopy (FESEM), atomic force microscopy (AFM), and RAMAN spectroscopy, were employed to analyze the film of AgNPs and AgNPs–PANI that was used to change the surface morphology of the screen-printed electrode (SPE). The various important parameters of effectiveness *viz.*, limit of detection (LOD) and limit of quantification (LOQ) for AgNPs–SPE and AgNPs–PANI–SPE were investigated and were found to be in the range of 5.3 mM, 16 mM and 2.5 mM, 7.4 mM, respectively, in PBS solution. Meanwhile, for the artificial saliva samples, the sensitivity of the AgNPs–PANI–SPE was obtained up to 0.00176 mA μM^{-1} cm^{-2} with an LOD of 0.76 mM. Furthermore, DFT results are used to examine the physical and electrical properties of the prepared functional films. The computing results show the functionalization of carbon with AgNP and AgNP–PANI, enabling a stable and reactive structure. The current research offers a non-enzymatic technique for precisely detecting LA biomolecules for medical applications.

Received 12th August 2024,
Accepted 9th December 2024

DOI: 10.1039/d4ma00813h

rsc.li/materials-advances

Introduction

Bio-sensing research for diverse metabolites has been performed previously for surveillance purposes such as clinical analysis, disease diagnosis, veterinary use, agricultural applications, industrial processing, environmental monitoring, *etc.*[1–5] Lactic acid is necessary for producing commercial dairy foods, medicinal items, chemical products, and cosmetics. It can be obtained from various sources, including plants, animals, and microbes. In addition, lactic acid can also be produced through the fermentation of carbohydrates.[6] Furthermore, lactic acid is essential and fundamentally required for the functioning and protection of the skin. It is essential in the food industry as a safe and effective preservative. As a result, lactic acid is an essential component in the processing of food, as well as its preservation.[7] In the human body, lactic acid is generated through physiological processes that occur under normal conditions, and it is frequently observed in various disease situations. Due to improper oxygen in the blood, anaerobic glycolysis occurs in the muscles and liver, producing lactic acid (LA), which has the chemical formula $C_3H_6O_3$.[8] Lactic acid at high concentrations can bring about a drop in blood pressure and a reduction in the amount of oxygen delivered to human tissues. Humans can feel the effects of these repercussions, including sepsis, heart attack, congestive heart failure, severe lung illness, respiratory failure, fluid accumulation in the lungs, and anemia.[9] Typical lactate concentrations are below 2 mM L^{-1}, whereas hyperlactatemia is characterized by lactate levels ranging from 2 mM L^{-1} to 4 mM L^{-1}.[10]

It has always been explained to us that sugar is the reason behind cavities, but the truth is that lactic acid causes the

[a] *Department of Mechanical Engineering, Indian Institute of Technology Jodhpur, 342030, Rajasthan, India. E-mail: ankurgupta@iitj.ac.in*
[b] *Healthcare Technology Innovation Centre, Indian Institute of Technology Madras, Chennai, Tamilnadu 600113, India*
[c] *Department of Electrical Engineering, Indian Institute of Technology Madras, Chennai, Tamilnadu 600036, India*

damage. In our mouths, a bacterium known as *Streptococcus mutans* is responsible for converting sugar to lactic acid, which erodes tooth enamel. The findings of the majority of studies indicate that, of the approximately 500 species of bacteria found in the mouth, *Streptococcus mutans* is responsible for the majority of decay.[11] Lactic acid is a prominent metabolic component found in the oral environment, occurring naturally in the human oral cavity as a byproduct of oral cell tissues and bacterial activity. The bacterial strain *Streptococcus mitis* can produce lactic acid. It is commonly found in dental plaque and has been identified as a causative agent in subgingival disorders.[12,13] Further studies show that the presence of lactic acid can accelerate the pitting corrosion in titanium dentures.[14] It is also observed that the salivary lactate levels exhibited a higher concentration among patients with septic shock than those without septic shock.[15] In this context, developing low-cost methods for monitoring lactic acid is essential. An effective and inexpensive technique for measuring lactic acid can be widely used for various purposes, including controlling the fermentation of lactic acid bacteria strains, which are typically used to create lactic acid, as well as for testing food, agricultural raw materials, *etc.*[16] High-performance liquid chromatography (HPLC) is the best procedure for measuring lactic acid, which includes ion–ion-pair, reversed-phase chromatography, and ion-exclusion.[17] HPLC is not often used in everyday practice since it requires expensive equipment, laborious sample preparation, and specialized personnel; the process is difficult, expensive, and labor-intensive.[18] Therefore, developing quick and accurate methods for measuring lactic acid is crucial.

The need for non-invasive, rapid, immediate, and cost-effective studies in human subjects is growing in significance, especially for individuals with blood collection challenges, such as hemophiliacs, neonates, and older people. The non-invasive collection of saliva to determine metabolites generally presents minimal challenges. However, the analysis may be complicated by bacteria, epithelial cells, and leukocytes. Electrochemical biosensors have demonstrated their efficacy in terms of specificity, selectivity, and user-friendliness in the quantification of metabolites for applications in clinical, environmental, and food analysis. One benefit of utilizing biosensors is the quick processing of the sample upon collection, without any separation procedures. Additionally, biosensors have a rapid response time, ranging from a few minutes to seconds. One notable feature is the high degree of specificity exhibited by the immobilized enzyme, coupled with the selectivity of the electrochemical transducer. This combination renders the probe well suited for conducting tests in biological fluids.

The sensitivity of the non-enzymatic biosensor can be improved by functionalizing the surface of the sensing material with specific molecules. The utilization of nanomaterials or nanostructures can significantly increase the surface area available for analyte binding. Nanoparticles, nanowires, and nanotubes can be utilized to enhance the signal by offering a substantial quantity of active sites for analyte interaction. Nanoparticles like carbon nanotubes (CNTs),[19,20] MXene,[21] gold nanoparticles (AuNPs),[22] platinum nanoparticles (PtNPs),[23] metal oxide-based nanoparticles like niobium oxide[24] or molybdenum oxide,[25] and semiconducting material-based nanoparticles like zinc oxide[26] all play essential roles in increasing the electrode surface area. Due to their electrochemical catalytic characteristics and excellent stability, transition metal oxides are highly desirable for developing non-enzymatic biosensors and other applications.[27–29] Electrochemical non-enzymatic LA detection methods always seek new materials and techniques to improve sensitivity and specificity. Silver nanoparticles (AgNPs), which have high electrical and optical properties, excellent biocompatibility and electrocatalytic activity, are among these metal nanoparticles.[30] Due to their unique features, conducting polymers[31] are incredibly popular among researchers and are a promising material. Polyaniline (PANI), a conducting polymer, has received much attention because of its vigorous redox activity, excellent thermal stability, and straightforward synthesis methods.[32–34] With the help of dopants or an oxidation–reduction reaction, its electrical conductivity can be easily adjusted.[35] It is possible to investigate the potential uses of this extraordinary property of PANI in microelectronics,[36] catalysis,[37] and sensing.[38,39] Fabricating electrode surfaces utilizing the emeraldine form of PANI opens a wide range of possibilities for detecting different biomolecules. It can be utilized as a diagnostic tool to predict the prognosis of various diseases.[40] PANI's inability to identify analytes at neutral pH and its limited activity in acidic pH (4) restrict its use in bio-electrochemistry.[41] The main methods used to address this problem are creating "self-doped PANI",[42] (ii) doping PANI with poly(acrylic acid) or poly(vinyl sulfonate),[43] and (iii) inserting gold nanoparticles (AgNPs) into the PANI matrix to increase the redox activity to close to neutral pH.[44]

In this work, lactic acid was directly electrochemically oxidized at the surface of AgNPs–SPE and Ag/PANI–SPE for non-enzymatic lactic acid detection. PANI has excellent optical/electronic properties, and good environmental stability, especially protonated/deprotonated properties and the addition of silver enhances the surface area for the adsorption of lactic acid. The sensing mechanism involves the oxidation of lactic acid molecules at the surface of the Ag/PANI electrode. A potential is applied to the Ag/PANI electrode in the presence of lactic acid molecules and lactic acid can adsorb onto the surface of the electrode. The adsorption of lactic acid molecules on an Ag/PANI electrode can modify its electronic structure and generate a local electric field that promotes the oxidation of lactic acid. Electrochemical oxidation involves the transfer of electrons from the lactic acid molecule to the electrode and the removal of hydrogen atoms from the lactic acid molecule. The protons produced in this reaction can react with the Ag/PANI electrode, leading to a change in the electrode potential and a corresponding change in the electrical current flowing through the electrode.

The current research aims to provide a quick, low-cost, and easy electrochemical approach for the detection of lactic acid by utilizing a functionalized layer of Ag and Ag–PANI over the screen-printed electrode, as shown in Fig. 1. The functionalized layer of AgNPs was developed through the drop-casting method, while for the Ag–PANI layer, electro-polymerization was done. Furthermore, these functionalized layers were characterized by

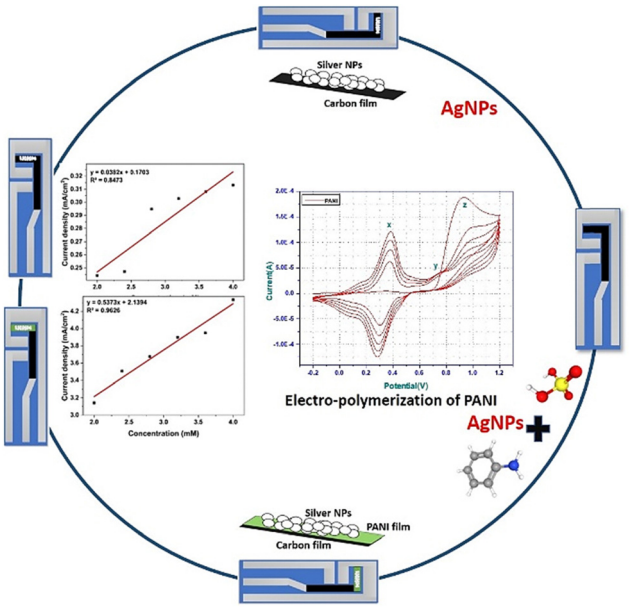

Fig. 1 A schematic view of the entire detection process.

FTIR, FESEM, AFM, and RAMAN spectroscopy. A brief comparison was done for both the functionalized layers to detect lactic acid. This technique helps to identify lactic acid in artificial saliva samples for medicinal applications and ensures good sensitivity, repeatability, and reproducibility.

Experimental

Materials

Analytical rank chemicals, including aniline (extra pure AR, 99.5%), potassium ferrocyanide (99%, $K_4[Fe(CN)_6]$), and potassium ferricyanide ($K_3[Fe(CN)_6]$) were purchased from Sisco Research Laboratories Pvt. Ltd, India. Lactic acid (LA), silver nitrate ($AgNO_3$), hydrochloric acid (HCl), and sulfuric acid (H_2SO_4) were purchased from Thermo Fisher India Pvt. Ltd. Ethanol was purchased from Changshu Hongsheng Fine Chemical Co. Ltd. Phosphate buffered saline was purchased from Sigma-Aldrich. Sodium borohydride was purchased from HiMedia Laboratories Pvt. Ltd, and ammonium persulfate from Fisher Scientific (India). The screen-printed electrodes (SPEs) used in this study were procured from Zimmer & Peacock (UK). The working area of 0.038 cm^2 of these SPEs consisted of carbon-paste material, in which Ag/AgCl was used to form the counter and reference electrode, respectively.

Characterization and sample preparation

Apparatus and measurements. Using a standard three-electrode system electrochemical workstation (ILMVAC GMBH, GERMANY, IVIUM State) with the SPE as the working electrode, all the electrochemical characterization/measurement and production of nanocomposite (Ag–PANI) were carried out. The electrochemical characterizations were performed using cyclic voltammetry (CV) experiments with a potential window of −0.2 to 1.2 V at a scan rate of 100 mV s^{-1}. All the investigations were carried out at room temperature. A Thermo Fisher Scientific Apreo 2S (15 kV-0.9 nm) microscope was used for topographical characterization utilizing field emission scanning electronic microscopy (FESEM) at low-vacuum mode with 10 kV acceleration voltages. Moreover, atomic force microscopy (AFM) in the non-contact mode was used to analyze the surface roughness of the modified SPE surface, and the pictures were then taken with a sophisticated scanning probe microscope (Park Systems XE-70, South Korea). FTIR spectrometer data was obtained from infrared measurements using Fourier transform IR (FTIR) spectroscopy (Vertex, 70 V + PMA50, Bruker, America), averaging over 32 scans. The FTIR spectra were obtained in transmission mode, with wavenumbers ranging from 500 to 4000 cm^{-1}. A twin-beam spectrophotometer (Varian, Cary 4000) was used for UV-visible spectroscopy. A Raman system (Bayspec, US) outfitted with a 532 nm laser generating about 30 mW of laser power at the sample was used to acquire the Raman spectra.

Preparation of silver nanoparticles

Fig. 2 shows the synthesis of a silver nanoparticle. The synthesis begins with the vigorous stirring of 0.002 M sodium borohydride ($NaBH_4$) in 30 ml of de-ionized (DI) water, which is then placed in an ice bath on a magnetic stirrer to regulate the final particle size and shape more effectively and to slow down the reaction. After 20 minutes, 2 mL of 0.001 M silver nitrate ($AgNO_3$) was added dropwise. Ag^+ ions were reduced and concentrated by combining the two solutions, resulting in monodispersed nanoparticles as a clear solution in an aqueous medium (*i.e.*, $NaBH_4$ and $AgNO_3$). As the nanoparticles combine, the suspension transforms from yellow to a deeper grey. The powder nanoparticles are obtained after the calcination of the slurry after drying it in an air oven for 60 minutes.[45]

Electro polymerization of aniline

A millimolar concentration of aniline monomer (0.5 mM) in 0.1 M H_2SO_4 was electro-polymerized utilizing a scan rate of 100 mV s^{-1} (*vs.* Ag/AgCl) in the potential range of 0.2 to 1.2 V. Thirty scan cycles were used to get an electrode surface with good electrocatalytic characteristics. A green hue was deposited on the SPE surface that matched the emeraldine form of PANI, named PANI/SPE. Furthermore, it was washed with DI water and kept in a freezer until needed.

Preparation of the Ag–PANI nanocomposite

Ag–PANI nanocomposite synthesis was formed by electropolymerization using the cyclic voltammetry technique. A solution containing a mixture of 2.5 mg of silver nanoparticles previously dispersed in aniline monomer (0.5 mM) in 0.1 M H_2SO_4 aqueous solution drop cast on (SPE) and electro polymerized utilizing at a scan rate of 100 mV s^{-1} (*vs.* Ag/AgCl) in the potential range of 0.2 to 1.2 V for 30 cycles.

Protocol for artificial saliva

Artificial saliva solution was prepared in DI water containing 4.27% sorbitol, 0.03% saccharin, 0.062% potassium chloride,

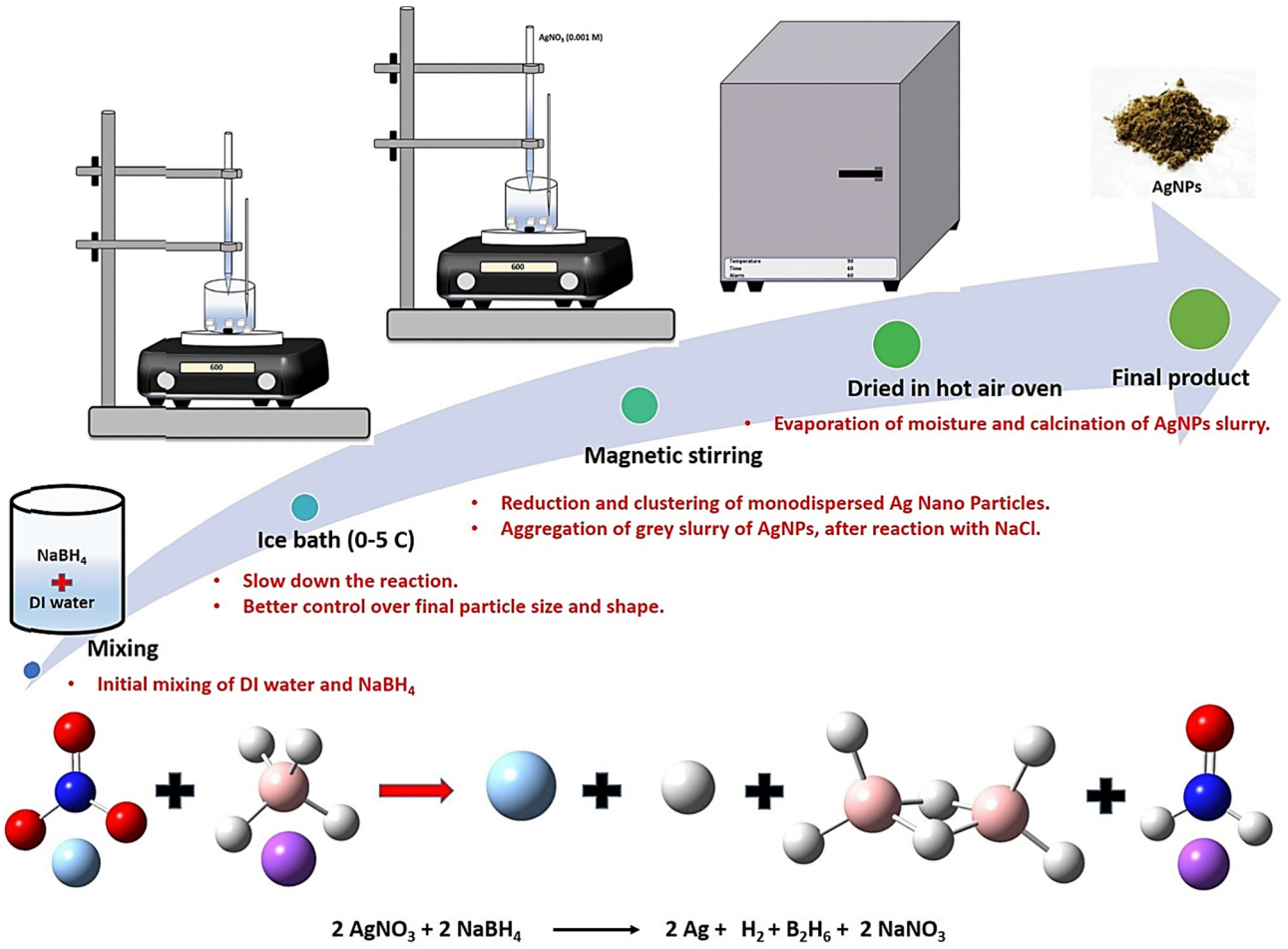

Fig. 2 Synthesis of silver nanoparticles.

0.086% sodium chloride, 0.012% magnesium chloride, 0.007% calcium chloride, 0.27% potassium phosphate monobasic, and 100 mL of DI water.[46]

Computational details

The energy calculations for the proposed structures, *viz.*, activated carbon (AC), lactic acid (LA), polyaniline (PANI), silver nanoparticles (AgNPs), AgNP–AC, and AgNP–PANI–AC, were performed using the density-functional theory (DFT) technique. The calculations were performed at the B3LYP level, employing the 6-31G and LANL2DZ basis sets.[47,48] Some parameters were derived from the computed structures, including the total energy (E), total dipole moment (TDM), and energy difference between the highest occupied molecular orbital (HOMO) and lowest unoccupied molecular orbital (LUMO) (*i.e.*, bandgap energy, ΔE).

Results and discussion

DFT calculations

Fig. 3(I) depicts the optimized molecular models of the proposed structures: AC, LA, and PANI with bond length. While Fig. 3(II) shows the optimized molecular model of Ag–AC and Ag–PANI–AC. It was observed that during the reaction between Ag–AC, the H–C═C bond increased from 1.38 Å to 1.42 Å, while the C═C bond increased from 1.36 Å to 1.41 Å. The same phenomena were observed for Ag–AC–PANI; when the Ag atom reacted with the AC–PANI structure, the N–H bond increased from 1.004 Å to 1.02 Å, while the Ag–H bond length was up to 2.92 Å. Table 1 presents a compilation of computed metrics, including energy, TDM, and HOMO/LUMO bandgap energy, indicating the chemical structure's physical and electrical properties. The total energy, which serves as a physical measure of the stability of the structure, is calculated as −16.6765, −17.1215, −9.3468, and −3.9663 keV for AC, PANI, LA, and AgNP, respectively.

The functionalization of AC with AgNP and AgNP–PANI leads to the formation of a composite material with significantly reduced energy levels of −20.6478 keV and −37.7730 keV, respectively. Consequently, this results in a notable increase in stability. TDM is widely regarded as a physical indication that reflects the reactivity of a structure. The computed values for the AC, PANI, LA, and AgNP materials are 4.2811, 0.5899, 2.1737, and 2.7755 Debye, respectively. AC's observed high reactivity could be attributed to its armchair configuration and the presence of six active sites, which results

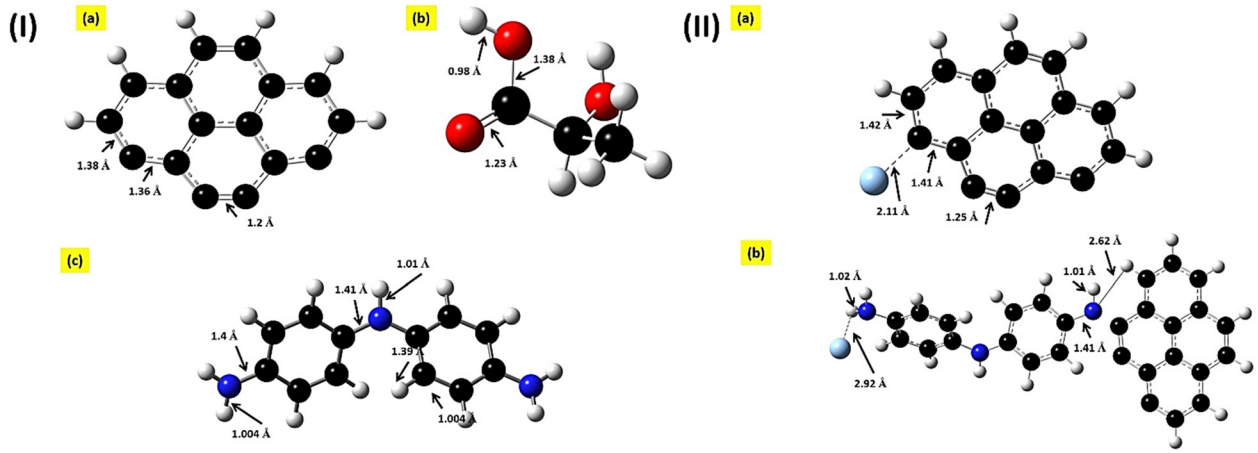

Fig. 3 (I) Optimized structures of (a) AC, (b) LA, and (c) PANI using DFT (*via* b3lyp/6-31g theoretical model), (II) optimized structures of (a) Ag–AC and (b) Ag–PANI–AC using DFT (*via* a b3lyp/lanl2dz theoretical model).

Table 1 Calculated total energy (E) in keV, total dipole moment (TDM) in Debye, and bandgap energy (ΔE) in eV for AC, PANI, LA, AgNPs, Ag–AC, and Ag–AC–PANI and their interaction possibilities using DFT: b3lyp/6-31g and the lanl2dz theoretical model

Structure	Total energy (E, keV)	TDM (Debye)	ΔE (eV)
AC	−16.6765	4.2811	0.7502
PANI	−17.1215	0.5899	4.3171
LA	−9.3468	2.1737	6.6573
AgNP	−3.9663	0	4.6627
AgNP–AC	−20.6478	2.6912	3.027
Ag–AC–PANI	−37.7730	4.9627	2.5304

from the removal of six hydrogen atoms from the lower positions of the molecular structure. The interaction between AgNP–AC exhibits a lower dipole moment of 2.6912, indicating lower reactivity.

On the other hand, AgNP–PANI–AC demonstrates a more significant dipole moment of 4.9627, suggesting increased reactivity compared to AC. The HOMO/LUMO bandgap energies are regarded as indicative of the electrical conductivity of the proposed structures. The energy (ΔE) change is measured to be 0.7502 eV for AC. In contrast, the PANI, LA, and AgNP values are 4.3171 eV, 6.6573 eV, and 4.6627 eV, respectively. However, the process of functionalizing activated carbon (AC) with silver nanoparticles (AgNP) and AgNP-polyaniline (AgNP–PANI) leads to an increase in the energy gap (ΔE) up to 3.027 eV and 2.5304 eV, respectively. Hence, the determined physical and electrical parameters establish the viability of functionalizing AC with AgNP and AgNP–PANI, enabling a stable and reactive structure.

Morphological and chemical characterization

Surface area (atomic force microscopy). When nanomaterials are employed to modify electrodes, there are various issues with utilizing the Randles–Sevcik equation to calculate the electrode surface area.[49] Atomic force microscopy (AFM) is used to calculate the surface areas of the various electrodes, including SPE, PANI–SPE, and Ag–PANI–SPE. For a 10 μm^2 representative region, the roughness of the three electrode samples has been determined. The 3D projections of the AFM are displayed in Fig. 4 XEI; the park system software is used to calculate the surface area (A) and the roughness, which are listed in Table 2.

The Ag–PANI film exhibits a higher surface area than the bare SPE by around 49.33%. The Ag–PANI composite and a few light agglomerations can be visualized in the FESEM images. The AgNPs were adequately covered with polymeric materials.

Structural characterization of SPE

Fig. 4(a–c) of the bare SPE, PANI, and Ag–PANI modified SPE confirm the efficacy of *in situ* electrosynthesis over the electrodes, and the FESEM pictures of the SPE surface revealed the presence of the Ag–PANI layer adhered to the working electrode. In contrast to the AgNP layer covering the electrode, it was found that the PANI development layer is uniform. Moreover, it produces a non-homogeneous layer on the surface, which can be seen in the AFM images. As shown in the exploded view of Fig. 4, AFM images also demonstrated an increase in roughness of approximately 17.6% for PANI and 49.33% for the Ag–PANI coated SPE compared to the bare SPE.

Functional group determination

Identifying functional groups in molecules using FTIR spectroscopy is possible because every chemical bond has a unique energy absorption band. To assess a complex's strength and type of bonds, it can also be used to learn about its structure and bonds.

Fig. 5 displays the FTIR spectrum of the AgNPs. The stretching of phenols by H–OH is demonstrated by the detection of bands at 3359 cm^{-1}. The stretching of the C–H of alkenes and alkyls was detected at 2856 and 2947 cm^{-1}, while C–H stretching of alkenes was observed at 3004 cm^{-1}. Aldehyde and ketone C=O stretching is indicated by the adsorption band at 1687 cm^{-1}. Peaks at 933, 827, and 711 cm^{-1} corresponding to C–H stretching of alkenes were detected. The bands seen at 1136

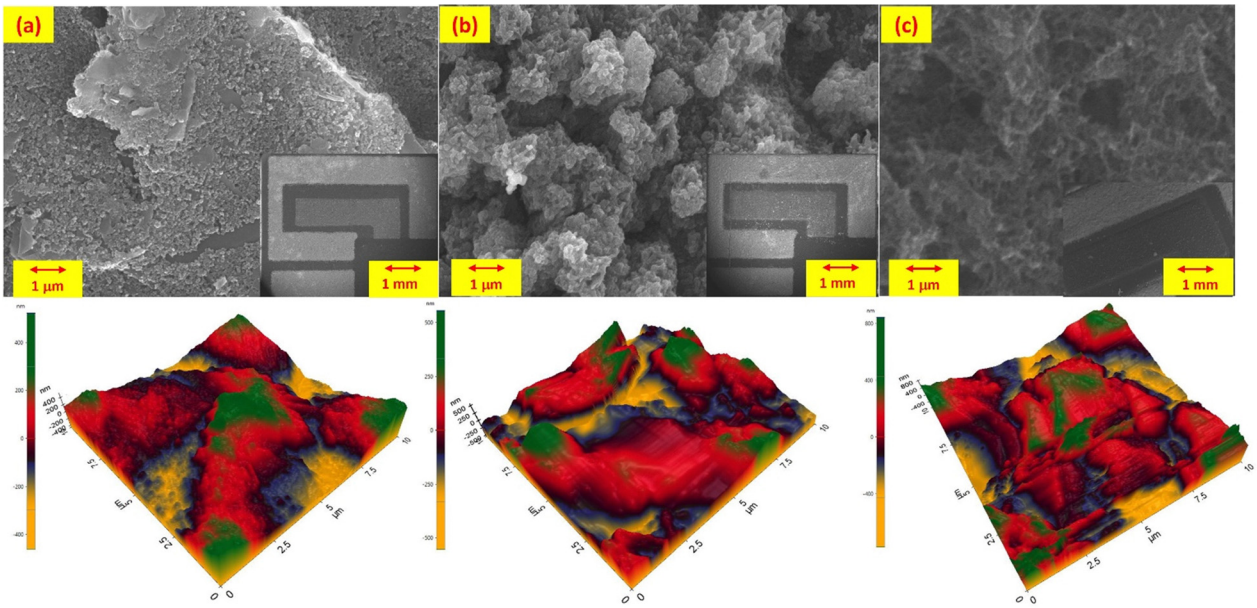

Fig. 4 FESEM images of the (a) bare, (b) PANI, and (c) Ag–PANI SPE surfaces, and an exploded view with an AFM micrograph.

Table 2 Roughness generated after surface modification of the SPE

Electrodes	Surface area (μm^2)	Roughness (nm)
SPE	10	117.187
PANI–SPE	10	137.811
Ag–PANI–SPE	10	175.724

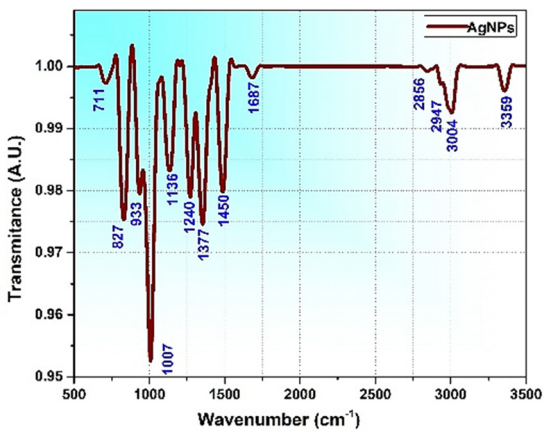

Fig. 5 FTIR spectra of silver nanoparticles.

and 1007 cm^{-1} show the stretching of esters along the C–O axis. The N═O symmetry stretching typical of the nitro compound is best seen in the band at 1377 cm^{-1}. The C–N stretching of amines is what causes the band at 1240 cm^{-1} to exist. The N–H stretch vibration occurring in the amide bonds of the proteins was ascribed to the band at 1450 cm^{-1}.[50]

Identification of molecules and intermolecular bonds

The vibrational modes of molecules are examined using the Raman spectroscopy method. Some of the light will be dispersed by a sample when it is exposed to a monochromatic light source. That scattered light can then be collected and analyzed to determine the molecular vibrations of the sample.

Fig. 6(a) shows a comparison of the Raman spectra of the bare SPE, PANI-modified SPE, and AgNP-modified SPE, which clearly shows effective functionalization of the working electrode layer. Meanwhile, Fig. 6(b) shows the Raman spectra of silver nanoparticles obtained using 532 nm excitation for 5 seconds at 30 mW power. The bands that were seen between 200 and 2200 cm^{-1} in the wavenumber range represent the stretching modes of different bonds. The vibrational maxima at 470 and 642 cm^{-1} are a result of the stretching vibration of C–N–C and C–S–C.[51] The other band, at wavelengths of 1284, 1364, and 1582 cm^{-1}, is produced by the carboxylic group symmetric and anti-symmetric C═O stretching vibrations, respectively.[52,53]

UV-vis of AgNPs

The ultraviolet-visible (UV-vis) absorbance spectra of the nanostructures of AgNPs were measured by dispersing them in deionized water using ultrasonic techniques. Fig. 7 shows the recorded spectra of AgNPs. The UV-visible absorption spectrum has a broad absorption peak at a wavelength of 406 nm, which is indicative of the presence of silver nanoparticles (AgNPs).[54]

Electrochemical characterization

Electro polymerization of aniline. Aniline was electro polymerized to create PANI films. Fig. 8 shows a typical CV growth of PANI film in aqueous 0.1 M H_2SO_4 + 0.5 mM aniline. A thin, uniform coating was developed on the electrode by continuous potential scanning at 100 mV s^{-1} in the potential range of 0.2 to 1.2 V. Peaks *x* through *z* indicate the formation of radical cations (peak *x*, 0.3 V), oxidation of head-to-tail dimers (peak *y*, 0.7 V), and

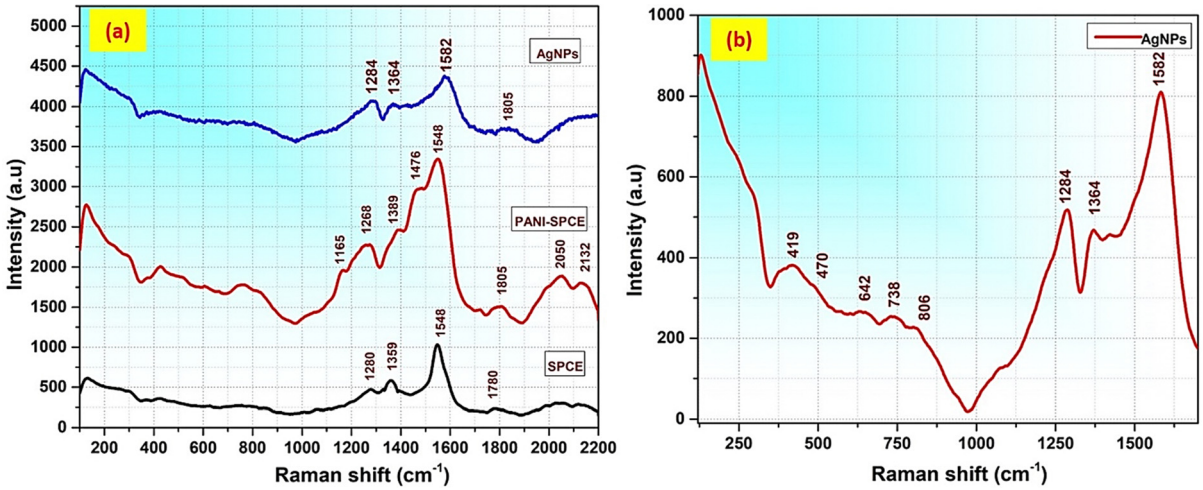

Fig. 6 Raman spectra for the modified SPE: (a) comparison of the modified surface of the SPE and (b) Raman spectra of AgNPs.

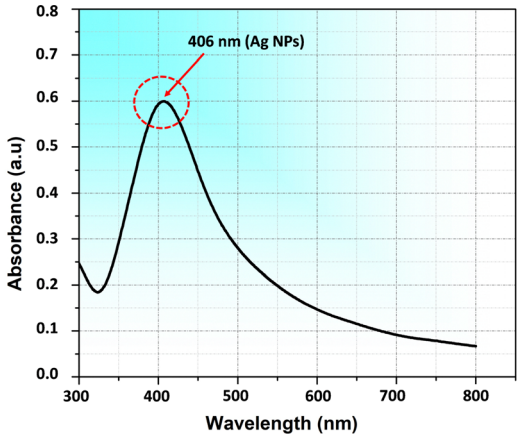

Fig. 7 UV absorption spectral analysis for the silver material.

the transition from the emeraldine to the pernigraniline structure (peak *z*, 0.9 V), respectively.[55,56] The fact that their peak heights increased with the number of potential cycles suggested that the films were both conductive and electroactive.

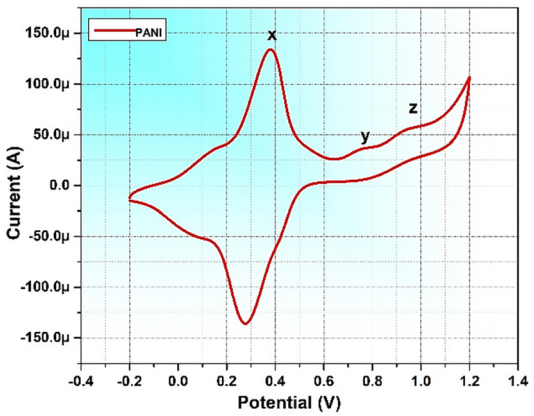

Fig. 8 Electro polymerization of aniline.

Effect of scan rate. The electrochemical kinetics of the lactic acid in the 4.0 mM PBS solution were investigated by measuring the CV response of lactic acid using an AgNPs and AgNPs–PANI modified screen-printed electrode (SPE) at varying scan speeds (20–100 mV s^{-1}). Fig. 9(a) shows the CV response of the AgNPs–SPE in a 4.0 mM lactic acid in PBS solution. Fig. 9(b) shows the CV response of the AgNPs–PANI–SPE in a 4.0 mM lactic acid in PBS solution. The most significant drop in peak current was noted when the scan rate was adjusted to 100 mV s^{-1}, as the scan rate approaches the positive and negative quadrants, the anodic and cathodic peak potentials change, which raises the possibility of a charge transfer kinetic limit. As the scan rates increased, the oxidation and reduction peaks, respectively, migrated to the right and left, as seen in Fig. 9(b). The relationship between the cathodic and anodic peak current ratios was consistent with the characteristics of surface-bound redox sites. The increased current density at higher scan rates confirms the AgNPs–PANI–SPE's catalytic activity for lactic acid detection. The well-defined CV curves for the AgNPs–PANI–SPE were achieved with a diffusion-controlled redox procedure.

Electrochemical behavior of SPE, PANI–SPE, and Ag–PANI–SPE. Fig. 10 shows the cyclic voltammetry response of a bare SPE, an Ag-modified SPE, and an Ag–PANI-modified SPE with 4.0 mM lactic acid in PBS solution at 100 mV s^{-1}. A simultaneous increase in the current density of the working

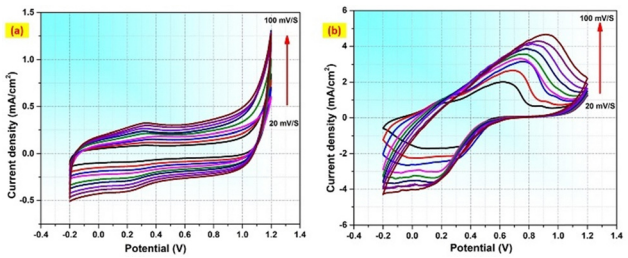

Fig. 9 CV analysis of 4.0 mM lactic acid in PBS solution at different scan rates: (a) Ag–SPE and (b) Ag–PANI–SPE.

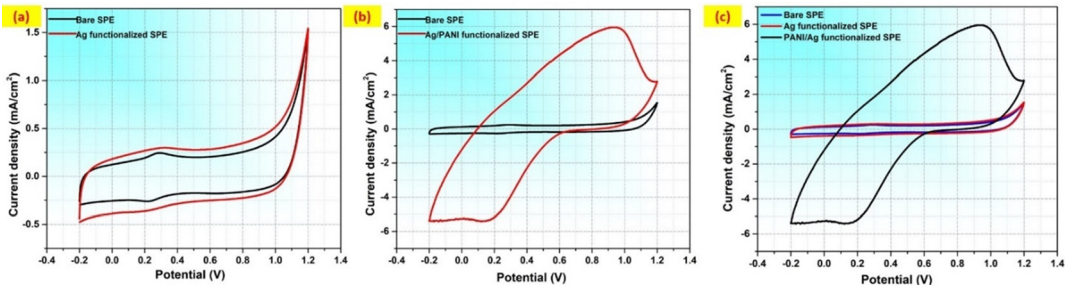

Fig. 10 Electrochemical behavior of (a) bare SPE and Ag-functionalized SPE, (b) bare SPE and PANI/Ag functionalized SPE, and (c) comparative graph of (a) and (b) for 4.0 mM lactic acid in PBS solution at 100 mV s^{-1} for the potential range of −0.2 to 1.2 V.

electrode was observed due to silver nanoparticles, as shown in Fig. 10(a). This can be attributed mainly to the large surface area to volume ratio, and the electronic properties of the AgNPs. Furthermore, it was observed that the anodic peak potentials of lactic acid occurred at a potential of around 0.3 V, and the evident peak currents provided convincing proof of the catalytic role played by AgNPs in the electro reduction of lactic acid. Furthermore, the AgNPs–PANI functionalized electrode surface, produces a sharp increase in current density, as shown in Fig. 10(b). A thin coating of PANI (a conducting polymer) formed electrochemically over the working electrode's surface, increasing the electrode's sensitivity for the detection of lactic acid. As the AgNPs–PANI functionalization layer develops over the working electrode, it increases the available surface area for electrochemical reactions, as shown in Fig. 4. This can lead to an increase in the current density observed in the CV graph Fig. 10(b); Fig. 10(c) shows a comparison between modified and bare electrodes.

Lactic acid detection. Fig. 11 shows the linearity curve with increasing concentration in PBS solution. Fig. 11(a) shows the linearity curve for AgNPs–SPE with increase in lactic acid concentration; it was observed that the produced current is positively and linearly related to the concentration of lactic acid with a R^2 value of 0.85. Fig. 11(b) shows the linearity curve for AgNPs–PANI–SPE with increase in lactic acid concentration; it was observed that the produced current is positively and linearly related to the concentration of lactic acid with a R^2 value of 0.96. As the concentration increased, the current increased as well, which confirms that the anodic (oxidation) peak increases with increasing analyte concentration, which is consistent with an increase in the oxidation of lactic acid molecules (inset Fig. 11(a and b)). It is observed that the limit of detection (LOD) for AgNPs–SPE and AgNPs–PANI–SPE was found to be 5.28 and 2.45 mM, respectively, while the limit of quantification (LOQ) was found to be up to 16.01 and 7.43 mM, respectively.

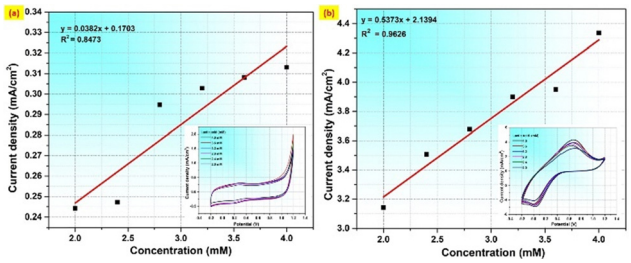

Fig. 11 Linearity curve with an increase in concentration: (a) Ag-functionalized SPE and (b) PANI/Ag functionalized SPE, for 4.0 mM lactic acid in PBS solution at 100 mV s^{-1} for the potential range of −0.2 to 1.2 V.

Artificial saliva sample testing. The artificial saliva samples were spiked with lactic acid with a wide range of concentrations (pH value 7.4) for further analysis of the functionalized electrode. The AgNP–PANI–SPE-based lactic acid sensor's chronoamperometric response is shown in Fig. 12(a). The enhanced performance of the modified electrode can be attributed to the higher concentration of LA, ranging from 50 μM to 4.0 mM, which directly leads to an increase in the conductivity of the catalyst. The catalyst functionalized over the working electrode has a robust electrocatalytic activity, which can be attributed to the relatively short response time of 5–15 seconds observed for lactic acid within the specified linear range. Fig. 12(b) illustrates the calibration curve depicting the relationship between lactic acid concentration and the corresponding current density response of the electrode modified with AgNP–PANI.

The evaluation of the limit of detection (LOD) was conducted using the $3.3 \times \frac{\text{Standard deviation of intercept}}{\text{Slope}}$ approach. The calibration plot revealed an estimated limit of detection (LOD) of 0.76 mM for lactic acid in artificial saliva samples. Fig. 12(c) shows consecutive readings of the same electrode for 2.0 mM concentration in artificial saliva. The functionalized SPE was used three times to verify the repeatability. Furthermore, Fig. 12(d) shows the consistency of the modified electrodes for 2.0 mM concentration in artificial saliva for three different electrodes.

Conclusion

In summary, this research elucidates the efficacy of AgNPs–PANI in the modification of SPE, leading to the development of a novel non-enzymatic sensor capable of detecting lactic acid.

- The electro polymerization approach was employed to successfully generate a functionalized layer of AgNPs–PANI over the working electrode of the SPE. An investigation was conducted to assess the effectiveness of the functionalized electrode by performing a cyclic voltammetry (CV) experiment using

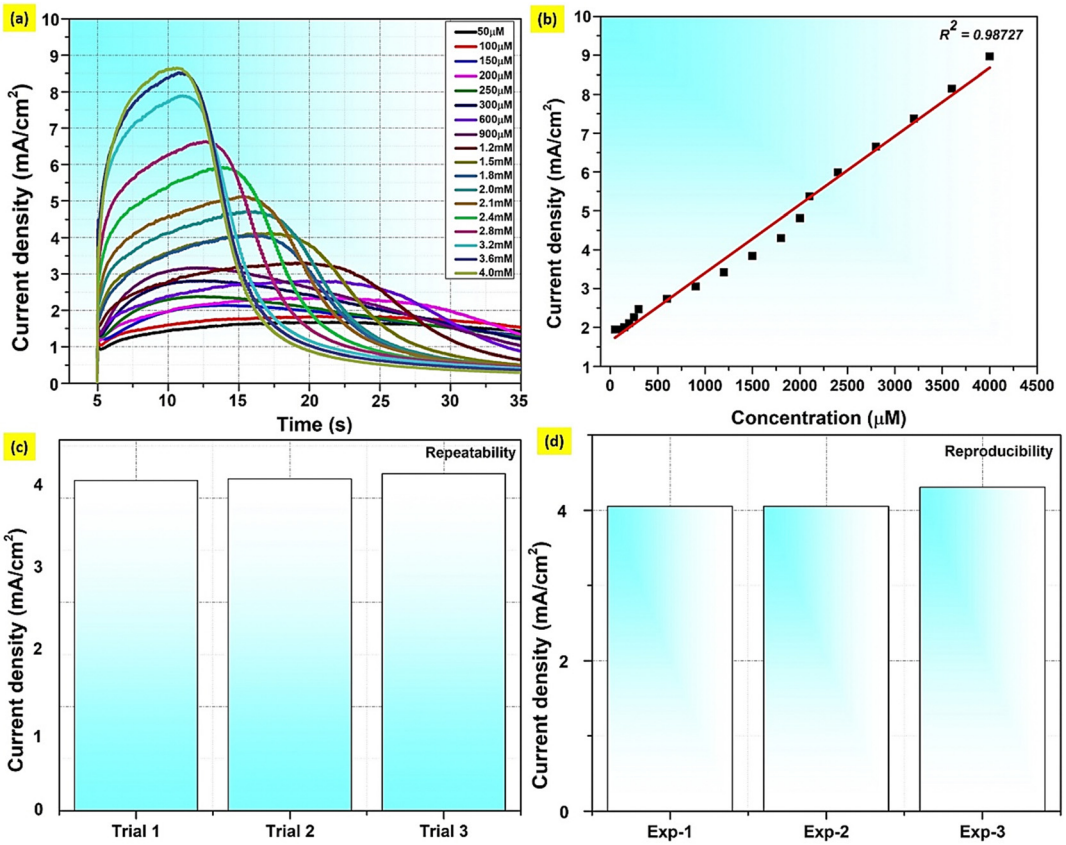

Fig. 12 Chronoamperometric responses of non-enzymatic sensing of lactic acid: (a) chronoamperometric sensing of different concentrations of lactic acid in an artificial saliva sample, (b) calibration plot at different concentrations, (c) repeatability of 2.0 mM lactic acid in artificial saliva and (d) reproducibility of 2.0 mM lactic acid in artificial saliva.

Table 3 A comparison of different sensing electrode materials for the L-lactic acid sensor using an electrochemical technique

Sensor type	Electrode materials	Linear range	Limit of detection	Sensitivity	Response time (s)	Sample
Non-enzymatic	Pt@chitosan/ $ZnTiO_3$NCs/GCE[57]	0.3–1.2 mM	22.36 μM	0.453 μA μM^{-1} cm^{-2}	—	Real sample
Non-enzymatic	WS_2/CO_3O_4/SPCE[58]	50–1000 μM	6 μM	—	5	0.1 M NaOH
Non-enzymatic	CuO/GCE[59]	0.05–40 mM	0.04 mM	14.47 mA mM^{-1} cm^{-2}	<5	Artificial sweat
Non-enzymatic	MWCNT-polypyrrole core–shell nanowire[60]	1–15 mM	0.051 mM	0.0029 mA mM^{-1} cm^{-2}	—	0.1 M Na_2SO_4
Enzymatic	ZnO nanotetrapods	0.0036–0.6 mM	0.0012 mM	0.028 mA mM^{-1} cm^{-2}	10	PBS
Non-enzymatic	MoS_2-AuPt[61]	0.005–3 mM	0.00033 mM	—	15	Sweat
Non-enzymatic	NiO NPs/GCE[62]	0.005–5 mM	0.0057 mM	—	—	0.1 M NaOH
Enzymatic	$H_2Ti_3O_7$ nanotubes[63]	0.5–14 mM	0.2 mM	0.24 μA mM^{-1} cm^{-2}	5	—
Non-enzymatic	3-aminophenylboronic acid (3-APBA)[64]	3–100 mM	1.5 mM	—	2–3 min	Sweat
Enzymatic	Polypyrrole-enzyme-CNT[65]	—	0.01 mM	—	—	—
Enzymatic	MWCNT-PTNPs[66]	0.2–2.0 mM	—	6.36 μA mM^{-1} cm^{-2}	5	Serum
Enzymatic	Electrode arrays by hydrogel photolithography[67]	0–10 mM	—	1.1 μA mM^{-1} cm^{-2}	—	—
Enzymatic	Pt–Ag thin film[68]	0.5–20 mM	—	2 nA mM^{-1}	2 min	—
Enzymatic	Nafion-Lox-PT working electrode[69]	50–350 μM	31 μM	0.04 μA μM^{-1} cm^{-2}	3 min	Food product
Non-enzymatic	Ag–PANI SPE (This work)	50 μM–4.0 mM	0.76 mM	0.00176 mA μM^{-1} cm^{-2}	5–15 s	Artificial saliva

an AgNPs and AgNPs–PANI modified-SPE in PBS solution, and further in artificial saliva samples. The enzyme-free sensor that has been proposed demonstrates a linear relationship between lactic acid concentration and its responses. It offers convenience in its usage, and exhibits a high level of sensitivity. The electrochemical experiments conducted in this study

demonstrated that the modified AgNPs–PANI–SPE exhibited a significant electrocatalytic capability for both the oxidation and reduction reactions of lactic acid. The current study primarily focuses on the typical range of lactic acid concentration in artificial saliva samples. As a result, this research holds considerable potential as a non-invasive method for detecting lactic acidosis caused by medical conditions. As per the results obtained, the limit of detection (LOD) for AgNPs–SPE and AgNPs–PANI–SPE was found to be 5.28 and 2.45 mM, respectively, in PBS solution. While for the artificial saliva samples, the sensitivity of Ag–PANI–SPE obtained was up to 0.00176 mA μM^{-1} cm^{-2} with LOD of 0.76 mM. It can be concluded that Ag–PANI–SPE is more sensitive and effective in comparison to Ag–SPE. Therefore, Ag–PANI–SPE provides good electronic properties and stability for better results.

• Furthermore, compilation of computed metrics, including energy, TDM, and HOMO/LUMO bandgap energy, indicates that functionalization of AC with AgNP–PANI leads to the formation of a composite material with significantly reduced energy levels of −37.7730 keV, increased dipole moment 4.9627 Debye, and increased energy gap (ΔE) 2.5304 eV, respectively. Hence, the determined physical and electrical parameters establish the viability of functionalizing AC with AgNP and AgNP–PANI, enabling a stable and reactive structure.

• In comparison to conventional techniques for detecting lactic acid, screen-printed electrode (SPE) based biosensing devices would provide several benefits, including affordability, compactness, and increased sensitivity along with the creation of compact, portable lab-on-the-go lactic acid analyzers for a variety of samples, including biological fluids and food samples. The reported Ag–PANI-modified SPEs have enormous potential to detect other analytes besides lactic acid (Table 3).

Author contributions

Conceptualization, A. G. and V. K.; methodology, V. K.; validation, V. K.; formal analysis, V. K. and R. A. M.; investigation, V. K. and R. A. M.; resources, A. G and S. N.; data curation, V. K.; writing – original draft preparation, V. K.; writing – review and editing, V. K. and A. G.; visualization, V. K.; supervision, A. G.; project administration, A. G.; funding acquisition, A. G., S. N., J. J. All authors have read and agreed to the published version of the manuscript.

Data availability

Data will be made available based on the request.

Conflicts of interest

There are no conflicts to declare.

Acknowledgements

The corresponding author wishes to acknowledge the Start-up Research Grant (SRG/2020/001895) provided by Science and Engineering Research Board, Department of Science and Technology, India and Healthcare Technology Innovation Center, Indian Institute of Technology, Madras for partial funding the research.

References

1 V. Kishnani, S. Kumari and A. Gupta, *Biosensors*, 2022, **12**, 1008.
2 V. Kishnani and A. Gupta, *ACS Appl. Bio Mater.*, 2023, **6**(10), 4336–4344.
3 S. Imani, A. J. Bandodkar, A. M. V. Mohan, R. Kumar, S. Yu, J. Wang and P. P. Mercier, *Nat. Commun.*, 2016, **7**, 1–7.
4 V. Kishnani, S. Park, U. T. Nakate, K. Mondal and A. Gupta, *Biomed. Microdevices*, 2021, **24**, 1–24.
5 V. Kishnani and A. Gupta, *2023 16th Int. Conf. Sens. Technol.*, 2023, 1–6.
6 P. Filannino, R. Di Cagno and M. Gobbetti, *Curr. Opin. Biotechnol*, 2018, **49**, 64–72.
7 S. C. Tang and J. H. Yang, *Molecules*, 2018, **23**, 863.
8 S. Forouzanfar, F. Alam, I. Khakpour, A. R. Baboukani, N. Pala and C. Wang, *IEEE Sens. J.*, 2020, **20**, 8965–8972.
9 R. Park, *West. J. Med.*, 1980, **133**, 418–424.
10 C. D. Foucher and R. E. Tubben, *StatPearls Publishing*, 2024, **https://www.ncbi.nlm.nih.gov/books/NBK568747/**.
11 **https://www.research.ufl.edu/publications/explore/v09n2/feature_03.html**, (accessed 3 August 2023).
12 L. Mikkelsen, E. Theilade and K. Poulsen, *Oral Microbiol. Immunol.*, 2000, **15**, 263–268.
13 P. A. Mashimo, Y. Yamamoto, M. Nakamura, H. S. Reynolds and R. J. Genco, *J. Periodontol.*, 1985, **56**, 548–552.
14 Q. Qu, L. Wang, Y. Chen, L. Li, Y. He and Z. Ding, *Materials*, 2014, **7**, 5528–5542.
15 D. K. Shruthi, S. M. Channabasappa, K. M. Mithun, B. S. Suresh, A. S. Tegginamani and T. Smitha, *J. Oral Maxillofac. Pathol.*, 2021, **25**, 437.
16 P. Lavermicocca, C. Reguant and J. Bautista-Gallego, *Front. Microbiol.*, 2021, **12**, 1946.
17 S. M. Ameen and G. Caruso, Chemistry of Lactic Acid, in *Lactic Acid in the Food Industry*, SpringerBriefs in Molecular Science, Springer, Cham, 2017, pp. 7–17.
18 R. Michalski, P. Pecyna-Utylska and J. Kernert, *Crit. Rev. Anal. Chem.*, 2020, **51**, 549–564.
19 L. Agüí, M. Eguílaz, C. Peña-Farfal, P. Yáñez-Sedeño and J. M. Pingarrón, *Electroanalysis*, 2009, **21**, 386–391.
20 M. Geetha, G. G. Nair, K. K. Sadasivuni, S. Al-maadeed and A. G. A. Muthalif, *Macromol. Symp.*, 2023, **412**, 2200150.
21 L. Lorencova, K. K. Sadasivuni, P. Kasak, J. Tkac, L. Lorencova, K. K. Sadasivuni, P. Kasak and J. Tkac, *Electroanalysis*, 2019, **31**(10), 1833–1844.
22 B. K. Jena and C. R. Raj, *Electroanalysis*, 2007, **19**, 816–822.

23 Y. Yu, Y. Yang, H. Gu, T. Zhou and G. Shi, *Biosens. Bioelectron.*, 2013, **41**, 511–518.
24 A. C. Pereira, A. Kisner, C. R. T. Tarley and L. T. Kubota, *Electroanalysis*, 2011, **23**, 1470–1477.
25 I. Shakir, M. Shahid, H. W. Yang, S. Cherevko, C. H. Chung and D. J. Kang, *J. Solid State Electrochem.*, 2012, **16**, 2197–2201.
26 Y. T. Wang, L. Yu, J. Wang, L. Lou, W. J. Du, Z. Q. Zhu, H. Peng and J. Z. Zhu, *J. Electroanal. Chem.*, 2011, **661**, 8–12.
27 V. Kishnani, K. Mondal and A. Gupta, *Met. Oxides Biomed. Biosens. Appl.*, 2022, 169–182.
28 M. Islam, K. Mondal, V. Kishnani, A. Gupta and A. Sharma, *Next Nanotechnol.*, 2024, **5**, 100057.
29 V. Kishnani and A. Gupta, *Impedance Spectroscopy and its Application in Biological Detection*, 2023, pp. 107–130.
30 C. A. Donini, M. K. L. da Silva, R. P. Simões and I. Cesarino, *J. Electroanal. Chem.*, 2018, **809**, 67–73.
31 H. Shirakawa, E. J. Louis, A. G. MacDiarmid, C. K. Chiang and A. J. Heeger, *J. Chem. Soc., Chem. Commun.*, 1977, 578–580.
32 K. Amano, H. Ishikawa, A. Kobayashi, M. Satoh and E. Hasegawa, *Synth. Met.*, 1994, **62**, 229–232.
33 J. G. Masters, Y. Sun, A. G. MacDiarmid and A. J. Epstein, *Synth. Met.*, 1991, **41**, 715–718.
34 J. C. Chiang and A. G. MacDiarmid, *Synth. Met.*, 1986, **13**, 193–205.
35 S. Bhadra, S. Chattopadhyay, N. K. Singha and D. Khastgir, *J. Appl. Polym. Sci.*, 2008, **108**, 57–64.
36 M. Angelopoulos, *IBM J. Res. Dev.*, 2001, **45**, 57–75.
37 S. Palaniappan and A. John, *Curr. Org. Chem.*, 2008, **12**, 98–117.
38 R. K. Pippara, P. S. Chauhan, A. Yadav, V. Kishnani and A. Gupta, *Micro Nano Eng.*, 2021, **12**, 100086.
39 V. Kishnani, G. Verma, R. K. Pippara, A. Yadav, P. S. Chauhan and A. Gupta, *Sens. Actuators, A*, 2021, **332**, 113111.
40 I. Lee, X. Luo, J. Huang, X. T. Cui and M. Yun, *Biosensors*, 2012, **2**, 205–220.
41 A. F. Diaz and J. A. Logan, *J. Electroanal. Chem. Interfacial Electrochem.*, 1980, **111**, 111–114.
42 J. Yue and A. J. Epstein, *J. Am. Chem. Soc.*, 1990, **112**, 2800–2801.
43 P. N. Bartlett, P. R. Birkin and E. N. K. Wallace, *J. Chem. Soc., Faraday Trans.*, 1997, **93**, 1951–1960.
44 S. Tian, J. Liu, T. Zhu and W. Knoll, *Chem. Commun.*, 2003, 2738–2739.
45 K. R. Mavani and Mihir Shah, *Int. J. Eng. Res. Sci. Technol.*, 2013, **2**(3).
46 L. F. de Castro, S. V. de Freitas, L. C. Duarte, J. A. C. de Souza, T. R. L. C. Paixão and W. K. T. Coltro, *Anal. Bioanal. Chem.*, 2019, **411**, 4919–4928.
47 M. Shukla, A. Verma, S. Kumar, S. Pal and I. Sinha, *Heliyon*, 2021, **7**, e06065.
48 V. Kishnani, A. Yadav, K. Mondal and A. Gupta, *Energies*, 2021, **14**, 5738.
49 T. R. L. C. Paixão, *ChemElectroChem*, 2020, **7**, 3414–3415.
50 K. Jyoti, M. Baunthiyal and A. Singh, *J. Radiat. Res. Appl. Sci.*, 2016, **9**, 217–227.
51 R. R. Arvizo, S. Bhattacharyya, R. A. Kudgus, K. Giri, R. Bhattacharya and P. Mukherjee, *Chem. Soc. Rev.*, 2012, **41**, 2943–2970.
52 D. Chen, X. Qiao, X. Qiu and J. Chen, *J. Mater. Sci.*, 2009, **44**, 1076–1081.
53 Y. F. Huang, H. T. Chang and W. Tan, *Anal. Chem.*, 2008, **80**, 567–572.
54 M. A. Khalilzadeh and M. Borzoo, *J. Food Drug Anal.*, 2016, **24**, 796–803.
55 E. M. Geniès, A. Boyle, M. Lapkowski and C. Tsintavis, *Synth. Met.*, 1990, **36**(2), 139–182.
56 E. M. Geniès, M. Lapkowski and J. F. Penneau, *J. Electroanal. Chem. Interfacial Electrochem.*, 1988, **249**, 97–107.
57 M. Faisal, M. M. Alam, J. Ahmed, A. M. Asiri, S. A. Alsareii, R. Saad Alruwais, N. Faihan Alqahtani, M. M. Rahman and F. A. Harraz, *J. Ind. Eng. Chem.*, 2023, **118**, 362–371.
58 G. Jeevanandham, G. P. Kuppuswamy, D. C. Sesu and K. Vediappan, *Surf. Interfaces*, 2023, **40**, 103097.
59 M. S. Sajna, J. J. Cabibihan, R. A. Malik, K. Kumar Sadasivuni, M. Geetha, J. Khalid Alahmad, D. Anwar Hijazi and F. Alsaedi, *Mater. Sci. Eng. B*, 2023, **288**, 116217.
60 Y. M. Choi, H. Lim, H. N. Lee, Y. M. Park, J. S. Park and H. J. Kim, *Biosensors*, 2020, **10**, 111.
61 H. Xiao, L. Cao, H. Qin, S. Wei, M. Gu, F. Zhao and Z. Chen, *J. Electroanal. Chem.*, 2021, **903**, 115806.
62 S. Amin, A. Tahira, A. Solangi, R. Mazzaro, Z. H. Ibupoto and A. Vomiero, *Anal. Methods*, 2019, **11**, 3578–3583.
63 M. Yang, J. Wang, H. Li, J. G. Zheng and N. Nick Wu, *Nanotechnology*, 2008, **19**, 075502.
64 N. V. Zaryanov, V. N. Nikitina, E. V. Karpova, E. E. Karyakina and A. A. Karyakin, *Anal. Chem.*, 2017, **89**, 11198–11202.
65 X. Cui, C. M. Li, J. Zang, Q. Zhou, Y. Gan, H. Bao, J. Guo, V. S. Lee and S. M. Moochhala, *J. Phys. Chem. C*, 2007, **111**, 2025–2031.
66 J. Huang, J. Li, Y. Yang, X. Wang, B. Wu, J. Ichi Anzai, T. Osa and Q. Chen, *Mater. Sci. Eng. C*, 2008, **28**, 1070–1075.
67 J. Yan, V. A. Pedrosa, A. L. Simonian and A. Revzin, *ACS Appl. Mater. Interfaces*, 2010, **2**, 748–755.
68 D. Pfeiffer, B. Möller, N. Klimes, J. Szeponik and S. Fischer, *Biosens. Bioelectron.*, 1997, **12**, 539–550.
69 O. Ozoglu, A. Uzunoglu, M. A. Unal, M. Gumustas, S. A. Ozkan, M. Korukluoglu and E. Gunes Altuntas, *J. Biosci. Bioeng.*, 2023, **135**, 313–320.